Journal of Proteomics xxx (xxxx) xxx–xxx

Contents lists available at ScienceDirect

Journal of Proteomics

journal homepage: www.elsevier.com/locate/jprot

Proteomic analysis reveals strong mitochondrial involvement in cytoplasmic male sterility of pepper (*Capsicum annuum* L.)

Jinju Guo, Peng Wang, Qing Cheng, Limin Sun, Hongyu Wang, Yutong Wang, Lina Kao, Yanan Li, Tuoyu Qiu, Wencai Yang, Huolin Shen*

Beijing Key Laboratory of Growth and Developmental Regulation for Protected Vegetable Crops, Department of Vegetable Science, College of Horticulture, China Agricultural University, Beijing, China

ARTICLE INFO

Keywords:
Capsicum annuum L.
Label-free
Proteomic analysis
Cytoplasmic male sterility
Isogenic maintainer lines

ABSTRACT

Although cytoplasmic male sterility (CMS) is widely used for developing pepper hybrids, its molecular mechanism remains unclear. In this study, we used a high-throughput proteomics method called label-free to compare protein abundance across a pepper CMS line (A-line) and its isogenic maintainer line (B-line). Data are available via ProteomeXchange with identifier PXD006104. Approximately 324 differentially abundant protein species were identified and quantified; among which, 47 were up-accumulated and 140 were down-accumulated in the A-line; additionally, 75 and 62 protein species were specifically accumulated in the A-line and B-line, respectively. Protein species involved in pollen exine formation, pyruvate metabolic processes, the tricarboxylic acid cycle, the mitochondrial electron transport chain, and oxidative stress response were observed to be differentially accumulated between A-line and B-line, suggesting their potential roles in the regulation of pepper pollen abortion. Based on our data, we proposed a potential regulatory network for pepper CMS that unifies these processes.

Biological significance: Artificial emasculation is a major obstacle in pepper hybrid breeding for its high labor cost and poor seed purity. While the use of cytoplasmic male sterility (CMS) in hybrid system is seriously frustrated because a long time is needed to cultivate male sterility line and its isogenic restore line. Transgenic technology is an effective and rapid method to obtain male sterility lines and its widely application has very important significance in speeding up breeding process in pepper. Although numerous studies have been conducted to select the genes related to male sterility, the molecular mechanism of cytoplasmic male sterility in pepper remains unknown. In this study, we used the high-throughput proteomic method called "label-free", coupled with liquid chromatography-quadrupole mass spectrometry (LC–MS/MS), to perform a novel comparison of expression profiles in a CMS pepper line and its maintainer line. Based on our results, we proposed a potential regulated protein network involved in pollen development as a novel mechanism of pepper CMS.

1. Introduction

Cytoplasmic male sterility (CMS) naturally occurs in numerous plant species, and it is characterized by normal vegetative organs but dysfunctional male gametes (pollen). This maternally inherited agronomic character has been widely used for commercial hybrid-seed production and for seedless fruit production [1]. Mitochondrial DNA dysfunction (abnormal recombination) is popularly hypothesized to be the cause of CMS. In many cases, male sterility can be restored specifically with restorer genes (*Rfs*) in the nucleus [2]. Indeed, previous studies have closely linked key mitochondrial processes (e.g., tricarboxylic acid cycle [TCA], respiratory electron transfer, and ATP synthesis) with male sterility [3–5].

Moreover, CMS-determining mitochondrial genes have been found in various plants; some of these genes appear to be chimeric, characterized as having open reading frames (ORFs) with segments from the mitochondrial genome or unknown sequences [6,7]. One example is the CMS-related gene T-*urf13* in maize [8], located upstream of the mitochondrial gene *orf221* (ATP4) [9,10]. A 5-bp insertion results in a frameshift mutation of *urf13*, ultimately causing male sterility [11]. Similarly, the petunia CMS-associated gene *pcf* is a chimeric gene originating from an aberrant recombination of the mitochondrial genome [12,13]. These CMS-related *orfs* are often located in or near ATP synthase subunits [14] and segments of cytochrome-oxidase subunit genes [15], e.g., *apt8* in sunflower [16–18], *apt9* in wheat and maize [19], *orf288* and *orf108* in *Brassica juncea* [20,21], as well as *WA352* in rice

* Corresponding author.
E-mail address: SHL1606@cau.edu.cn (H. Shen).

http://dx.doi.org/10.1016/j.jprot.2017.08.013
Received 20 April 2017; Received in revised form 12 August 2017; Accepted 18 August 2017

[22,23].

Other genes affected under CMS are those associated with pollen or anther development, specifically pollen exine formation. Exine is the outer coating of a pollen grain and is essential to viable pollen. It primarily consists of sporopollenin [24,25], a highly durable complex biopolymer comprising fatty acids, phenolics, and alkanes [26,27]. Thus, defects in sporopollenin biosynthesis affect pollen exine formation. For instance, *MS2* mutation-*male sterility 2* (*ms2*) mutants in *Arabidopsis* produce abortive pollen without an exine layer. *CYP704B* mutants in *Arabidopsis* [28] and rice [29] display immature microspores with aberrant pollen exine. Pollen grains of *lap*5 or *lap6* mutants exhibit abnormal exine patterning, while *lap5/lap6* double-mutant males have no exine and are entirely sterile [30].

Traditional two-dimensional electrophoresis (2-DE) has been widely applied to understand the mechanisms underlying CMS, revealing a network of male-sterility-related proteins in many plants and providing further insight on candidate genes related to male sterility [31]. In HL-type CMS rice, for example, functional classification of CMS-linked, differentially expressed proteins (DEPs) indicated an involvement in pollen developmental processes, including metabolism, protein biosynthesis, signal transduction, cell death, and energy production [32]. In pepper, analysis of anther proteomes between CMS and maintainer lines revealed that DEPs are potentially associated with instability in energy metabolism, excessive ethylene synthesis, or starch synthesis reduction [33]. Despite the identification of these CMS-associated sequences, exact CMS mechanisms remain controversial, because 2-DE cannot detect low-abundance, very large, or very small proteins [34]. Non-gel-based quantitative proteomic methods can overcome such shortcomings. In this study, we used the high-throughput proteomic method to perform a novel comparison of expression profiles in a CMS pepper line and its maintainer line to reveal a potential mechanism of pepper CMS.

2. Materials and methods

2.1. Plant materials

The CMS (A-line) and maintainer (B-line) lines selected for this study are similar in phenotype and genotype, differing only in fertility. Plants were grown in experimental fields of China Agricultural University, Beijing, China. Flower buds and anthers at different developmental stages were also collected for aceto-carmine staining and semi-thin paraffin section analysis with sarranine staining [35]. About 0.15 g FW (fresh weight) anthers at the tetrad stage (sepals wrapped corolla; vertical diameter, ~4.17 mm; transverse diameter, ~3.17 mm) were collected, frozen in liquid nitrogen immediately, and stored at − 80 °C. For proteomic, gene expression and physiological analysis, anthers were collected from 20 to 60 flower buds at the tetrad stage, which were selected randomly from 10 pepper plants. For morphological analysis, five flower buds at each development stage were collected from five pepper plants. The whole experiments were repeated three times.

2.2. Protein extraction

Frozen pepper anthers were ground in liquid nitrogen before the addition of 500 μL protein cracking liquid, containing 20 mM Tris-HCl (pH 7.5), 250 mM sucrose, 10 mM EGTA, 1% Triton X-100, protease-inhibitor mixture (cOmplete™), and 1 M DTT. The mixture was incubated on ice for 20 min, and then centrifuged at 15000*g* and 4 °C for 15 min. The supernatant was collected and the incubation-centrifugation was repeated. Protein quality was determined with SDS-PAGE. Protein concentration was determined with a BCA protein assay kit using BSA as a standard and a wavelength of 562 nm. Supernatants were stored at − 80 °C until use.

2.3. Label-free analysis

Protein samples were reduced with 1 M DTT for 1 h at 37 °C, alkylated with 1 M iodoacetamide (IAA) for 1 h in the dark, and then digested with sequencing-grade modified trypsin (Promega) for 20 h at 37 °C. Digested peptides were separated with chromatography using an Easy-nLC1000 system (Thermo Scientific) autosampler. Peptide mixture were loaded on a self-made C18 trap column (C18 3 μm, 0.10 × 20 mm) in solution A (0.1% formic acid), then separated with a self-made Capillary C18 column (1.9 μm, 0.15 × 120 mm) with a gradient solution B (100% acetonitrile and 0.1% formic acid) at a flow rate of 600 nL/min. The gradient consisted of the following steps: 0%–10% solution B for 16 min, 10%–22% for 35 min, 22%–30% for 20 min, then increasing to 95% solution B in 1 min, holding for 6 min. Separated peptides were examined in the Orbitrap Fusion mass spectrometer (Thermo Scientific) with a Michrom captive spray nano-electrospray ionization (NSI) source. Spectra were scanned over the m/z range 300–4000 Da at 120,000 resolution. 18 s exclusion time and 32% normalization collision energy were set at the dynamic exclusion window.

RAW files were extracted using the MASCOT version 2.3.02 (Matrix Science, London, UK) embedded into Proteome Discover 2.0 (Thermo Scientific). MS data were searched against a pepper genome database containing 35,336 sequences (http://peppersequence.genomics.cn/page/species/index.jsp). Parameters were set as follows: fully tryptic peptides with ≤ 2 missed cleavages were permitted; carbamidomethylation (C) and oxidization (M) were as fixed and variable modifications, respectively; peptide mass tolerance was 15 ppm, and fragment mass tolerance was 20 mmu; the charge state of the peptides were set from + 2 to + 6. The cutoff of global false discovery rate (FDR) for peptide and protein identification was set to 0.01.

Chromatographic peak intensity (peak area) was calculated and normalized by deviation coefficient. This deviation coefficient was calculated by dividing the maximum value of sum-peak area by the sum-peak area of samples [36]. Protein species with at least two unique peptides were selected for protein species quantitation, and the relative quantitative protein ratios between the two samples were calculated by comparing the average abundance values (three biological replicates). Student's *t*-tests were performed to determine the significance of changes between samples. A fold-change of > 2 and *P*-value < 0.05 in at least two replicates was used as the thresholds to define differently accumulated protein species. Additionally, protein species detected in only one material (A-line or B-line) with at least two replicates were considered to be presence/absence protein species. The correlation coefficient (R^2) between three biological replicates and the biological coefficient of variation (CV) of each protein species were also calculated [37].

2.4. Bioinformatics analysis

Bioinformatics analysis of proteins was performed according to Liu et al. [35]. Functional annotation and category analysis was performed using the online software Blast2GO (http://www.geneontology.org). Protein pathway analysis was performed using the Kyoto Encyclopedia of Genes and Genomes KEGG (http://www.genome.jp/kegg). A *P*-value ≤ 0.01 was used as the threshold to determine the significant enrichments of GO and KEGG pathways.

The mass spectrometry proteomics data have been deposited to the ProteomeXchange Consortium via the PRIDE partner repository with the dataset identifier PXD006104. The reviewer account: Username: reviewer66969@ebi.ac.uk; Password: muJIWrjs.

2.5. Quantitative real-time PCR (qRT-PCR) analysis

Total RNA was isolated from anthers with the SV Total RNA Isolation System Kit (Promega, USA), following manufacturer protocol. First-strand cDNA was synthesized with a PrimeScript™ RT Kit (Takara,

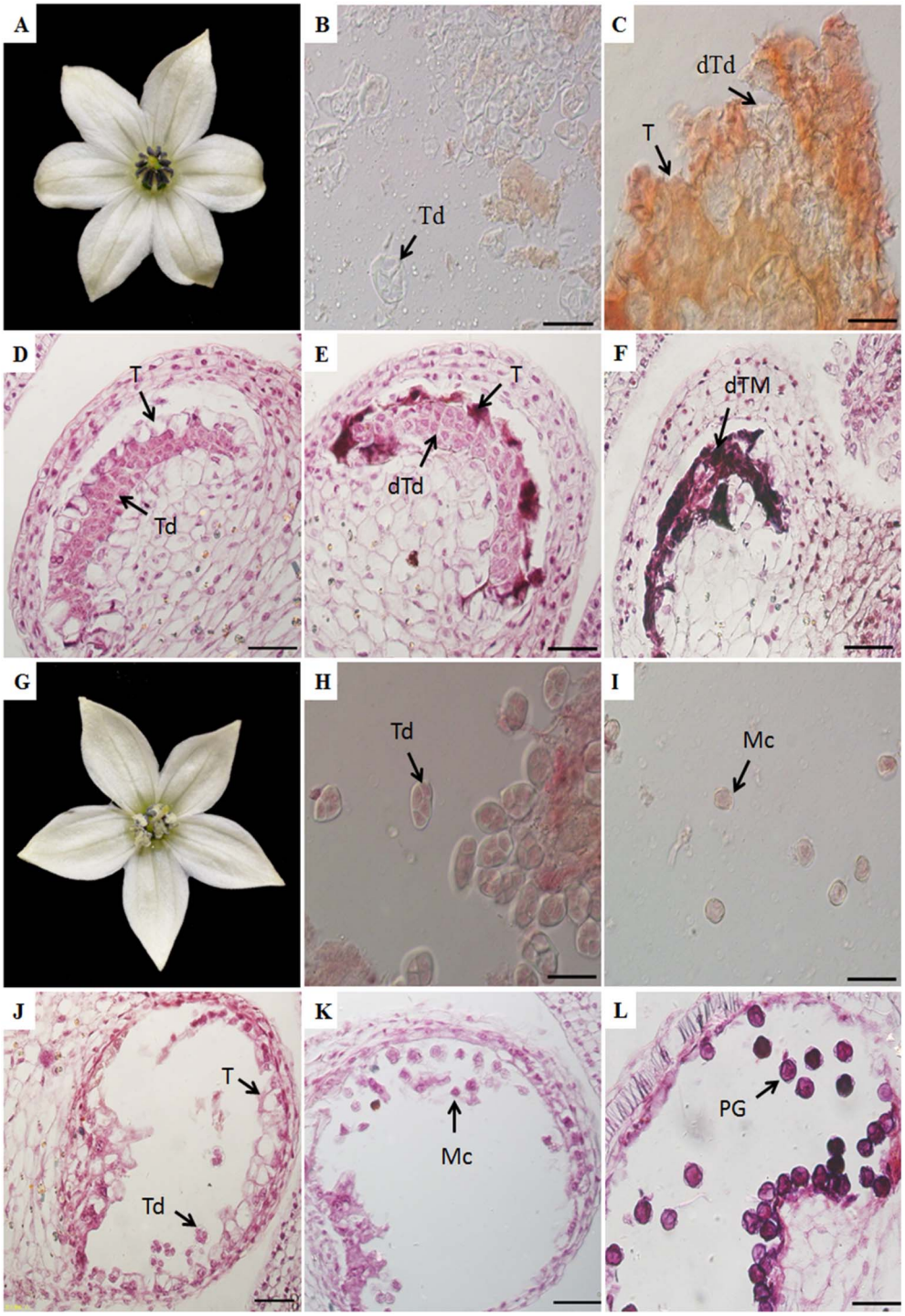

Fig. 1. Pollen morphological features in the CMS (A-line) (A–F) and the isogenic maintainer (B-line) (G–L). Acetocarmine (1%) staining of microspores (B, C, H, I) and paraffin section analysis of anthers (D–F, J–L). B, D, H, J at the tetrad stage; C, E, I, K at the uninucleate stage; F, L at mature stage. Td, tetrad; T, tapetum; Mc, microspore; dTd, death tetrad; dT, death tapetum; dTM, death tapetum and microspore; PG, pollen grain. Scale bars = 200 μm.

Japan). The qRT-PCR was performed with a GoTaq® qPCR Master Mix (Promega, USA), following manufacturer protocol, in an ABI 7500 real-time PCR system. The thermocycling conditions were set as follows: 95 °C for 1 min, 40 cycles of 95 °C for 15 s, and 60 °C for 1 min. Relative expression levels of target genes were calculated using the $2^{-\Delta\Delta Ct}$ method. qRT-PCR were conducted with three biological replicates and three technical replicates. Statistical analyses of data were carried out by ANOVA analysis and means were separated by the least significant difference (LSD) test at $P < 0.05$ and $P < 0.01$ level. All primers are listed in Supplementary Table 1.

2.6. Measurement of ROS contents and antioxidant enzyme activities

O_2^- levels were assayed using nitroblue tetrazolium (NBT), following Elstner and Heupel [38]. H_2O_2 content was determined with a ferric-xylenol orange hydroperoxide assay [39]. Lipid peroxidation levels were measured using barbituric acid (TBA) [40]. To determine the activity of antioxidant, about 0.25 g FW anthers were ground in cold extraction buffer containing 0.1 M Tris-HCl (pH 7.8), 0.5 M EDTA and 1% PVP. Homogenates were collected and centrifuged at 10,000*g* for 15 min at 4 °C. The supernatant was collected and used for assay of enzyme activities. Superoxide dismutase (SOD) activity was tested according to the methods of Giannopolitis and Ries [41].

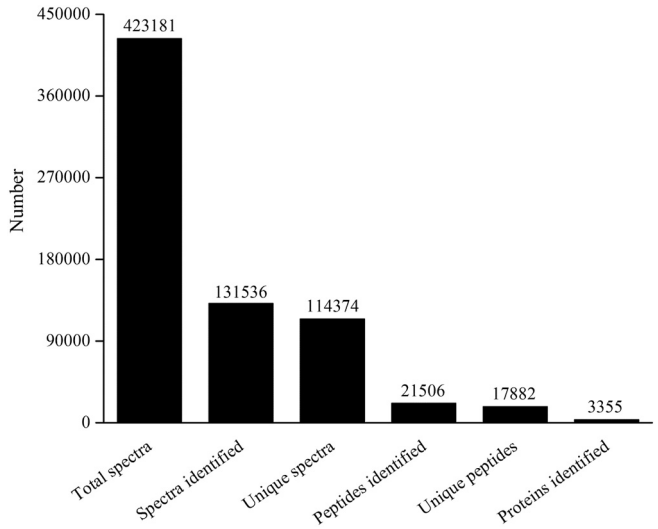

Fig. 2. Spectrum, peptides and proteins identified from label-free proteomics by searching against pepper database.

Guaiacolperoxidase (POD) activity was tested following Zheng and Huystee [42] method. Catalase (CAT) activity was estimated according to the method of Aebi [43]. Three biological replicates and three technical replicates were designed in this experiment. All data was presented as the mean ± SE values of each treatment. Similar significance analyses were conducted based on the description of qRT-PCR.

2.7. Enzyme linked immunosorbent assay (ELISA)

To validate the differently accumulated proteins, four enzymes involved in organic acid metabolism were measured by commercially available plant ELISA test kits (Future Industrial Limited by Share Ltd., Shanghai, China) following manufacturer's protocol. Samples were homogenized in 0.01 M phosphate buffer solution (PBS, pH = 7.4). Homogenates were collected and centrifuged at 5000*g* for 10 min at 4 °C. 50 μL diluted supernatants (1:5) were added per well, incubated at 37 °C for 30 min and then washed with 350 μL washing solution for 5 times. After drying, 50 μL antibody-enzyme (HRP) conjugate solutions were added per well, incubated at 37 °C for 30 min and washed 5 times. Substrate mixture (A and B) was pipetted into each well. After incubation at 37 °C for 15 min, the enzymatic reaction was stopped by adding 50 μL stopping buffer. Absorbance was assayed using an enzyme-labeling instrument (RT-6100, Rayto, USA) at 450 nm. Three biological replicates and three technical replicates were designed in this experiment.

2.8. High performance liquid chromatography (HPLC) analysis

A high performance liquid chromatography (HPLC) method was used to analyze the contents of organic acids (pyruvic acid, α-ketoglutaric acid and citric acid). For α-ketoglutaric acid and citric acid analysis, about 0.2 g FW anthers were ground and treated for 30 min with power ultrasound in 10 mM K_2HPO_4 (pH = 2.55) and incubated for 1 h at 60 °C. After centrifuged at 6000 r/min for 20 min and filtered through 0.45 μm Millipore filter, 10 μL supernatant was loaded on Thermo C18 column (250 × 4.6 mm, 5 μm). The mobile phase consisted of 10 mM K_2HPO_4 (pH = 2.55) at a flow rate of 0.5 ml/min. The measurements were operated at 210 nm with UV detection and the temperature is 30 °C. For pyruvic acid analysis, the mobile phase consisted of 0.5% $(NH_4)_2HPO_3$ (pH = 2.5) and acetonitrile in the ratio 95:5 (v/v). Three biological replicates were designed in this experiment.

3. Results

3.1. Pollen morphological features

Aceto-carmine staining and paraffin sections were used to define the development stage of microspores. Morphological differences between the CMS and maintainer lines during pollen abortion were observed at the tetrad stage (Fig. 1B, D, H, J). Tapetum is the innermost layer of the anther wall and surrounds the locule. Here, B-line tapetum cells were degraded for proper microspore development (Fig. 1J), while A-line tapetal cells exhibited vacuolation and premature death (Fig. 1D). Subsequently, A-line tapetal cells tightly surrounded and squeezed microspores, inhibiting callosum degradation and microspore release from the tetrad to the uninucleate stage (Fig. 1C, E), eventually causing microspore rupture and death at the late-uninucleate stage (Fig. 1F). Collapsed tapetal cells and crushed microspores ultimately formed a dense belt (Fig. 1F). Thus, premature tapetum death may be the cause of microspore abortion at the tetrad stage.

3.2. Primary data analysis and protein identification

The result of SDS-PAGE was exhibited in the Supplementary Fig. S1. A total of 423,181 spectra were generated using label-free experiment across the CMS and isogenic maintainer lines. A total of 131,536 spectra matched to known spectra, 114,374 unique spectra, 21,506 peptides, 17,882 unique peptides and 3355 protein species were identified (FDR ≤ 0.01) (Fig. 2, Supplemental Table 2). About 74% (2012 of 2732) and 80% (2126 of 2652) of proteins had a biological CV of < 30% in A-line and B-line, respectively. And the correlation coefficient (R^2) between biological replicates were 0.992 (A_1 & A_2), 0.991 (A_1 & A_3), 0.98 (A_2 & A_3), 0.995 (B_1 & B_2), 0.997 (B_2 & B_3), 0.995 (B_1 & B_3), respectively (Supplemental Table 2). The distribution of length of peptides and number of peptides defining each protein were provided in Figs. 3 and 4. Then, about 2594 (77%) unique proteins matched with at least two unique peptides were selected for further analysis (Fig. 4) and the distribution of these quantified protein species was showed as a volcano plot (Supplementary Fig. S2).

3.3. Analysis of differential abundance protein species (DAPS)

Based on the threshold for screening DAPS (i.e., fold-change of 2 and $P \leq 0.05$), 324 differentially abundant protein species were identified and quantified; 47 were up-accumulated and 140 were down-accumulated in the A-line. Additionally, 75 and 62 protein species specifically accumulated in the A- and B-lines, respectively (Fig. 5;

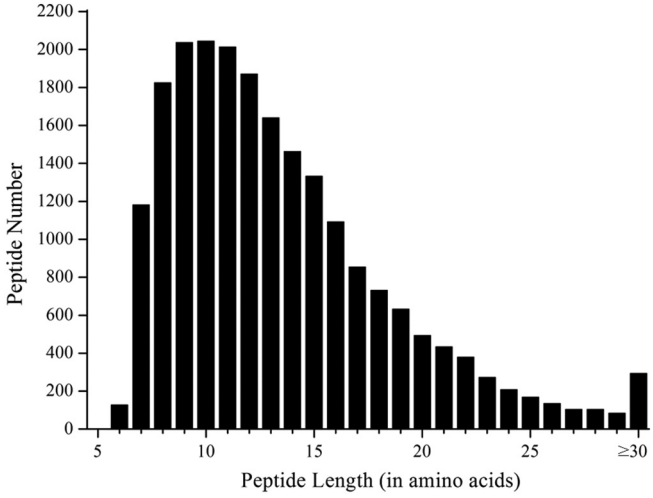

Fig. 3. The distribution of length of peptides.

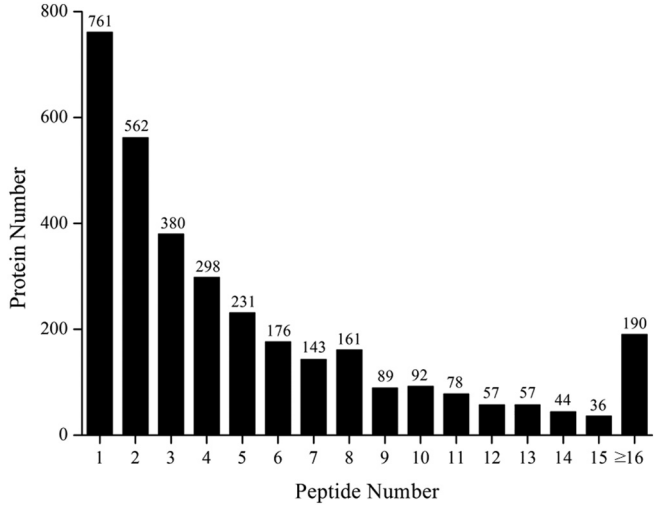

Fig. 4. Number of peptides that match to unique proteins number.

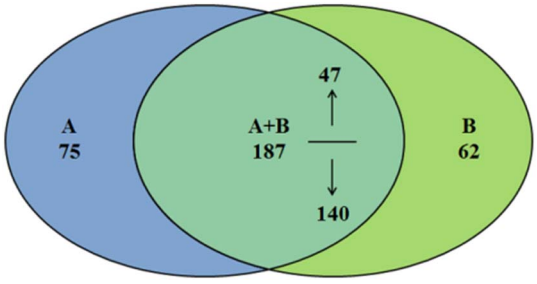

Fig. 5. Comparison of DAPS identified in the A-line (A) and B-line (B). "↑" and "↓" indicate up-accumulated and down-accumulated, respectively. "A + B" indicates the DAPS identified in both lines.

Supplementary Table 3). These large numbers imply a complex regulatory network for pollen abortion in pepper.

Gene ontology (GO) analysis indicated that protein species involved in pollen wall assembly and pollen exine formation were enriched at the tetrad stage ($P \leq 0.01$; Table 1). To further identify the significant difference of the pathway between A-line and B-line, we next performed KEGG pathway analysis on the identified DAPS. 143 (44.14%) DAPS were mapped to 58 pathways in the KEGG database. And detected DAPS were significantly enriched in five associated pathways ($P \leq 0.01$): stilbenoid, diarylheptanoid and gingerol biosynthesis ($P = 0.0039$), flavonoid biosynthesis ($P = 0.0064$), limonene and pinene degradation ($P = 0.0066$), phenylpropanoid biosynthesis ($P = 0.0082$), as well as pyruvate metabolism ($P = 0.0119$) (Table 2). Phenylpropanoid biosynthesis pathways have been previously associated with pollen exine formation [44–46], and the stilbenoid, diarylheptanoid and gingerol biosynthesis, flavonoid biosynthesis are part of phenylpropanoid biosynthesis pathways. Moreover, pyruvate metabolism supplies substrates for limonene and pinene degradation. In sum, the difference between A- and B-lines was mainly related to pollen exine formation and pyruvate metabolism.

Table 1
Gene ontology enrichment for the DAPS ($P \leq 0.01$).

GO: ID	Description	*P*-value
GO:0030198	Extracellular matrix organization	9.01E − 08
GO:0043062	Extracellular structure organization	9.01E − 08
GO:0010208	Pollen wall assembly	1.10E − 06
GO:0010584	Pollen exine formation	1.10E − 06
GO:0010927	Cellular component assembly involved in morphogenesis	1.10E − 06
GO:0085029	Extracellular matrix assembly	1.10E − 06
GO:0032989	Cellular component morphogenesis	6.15E − 06
GO:1901136	Carbohydrate derivative catabolic process	7.92E − 06
GO:0048869	Cellular developmental process	1.44E − 05
GO:0009555	Pollen development	1.48E − 05
GO:0048646	Anatomical structure formation involved in morphogenesis	3.59E − 05
GO:0048229	Gametophyte development	8.43E − 05
GO:0009653	Anatomical structure morphogenesis	1.32E − 04
GO:0016998	Cell wall macromolecule catabolic process	1.65E − 04
GO:0033609	Oxalate metabolic process	2.46E − 04
GO:0046564	Oxalate decarboxylase activity	2.46E − 04
GO:0080110	Sporopollenin biosynthetic process	5.17E − 04
GO:0045735	Nutrient reservoir activity	5.17E − 04
GO:0004743	Pyruvate kinase activity	1.24E − 03
GO:0030955	Potassium ion binding	1.24E − 03
GO:0031420	Alkali metal ion binding	1.24E − 03
GO:0044550	Secondary metabolite biosynthetic process	1.93E − 03
GO:0002682	Regulation of immune system process	1.97E − 03
GO:0006516	Glycoprotein catabolic process	1.97E − 03
GO:0031349	Positive regulation of defense response	1.97E − 03
GO:0045088	Regulation of innate immune response	1.97E − 03
GO:0050776	Regulation of immune response	1.97E − 03
GO:0045229	External encapsulating structure organization	2.03E − 03
GO:0044036	Cell wall macromolecule metabolic process	2.99E − 03
GO:0006026	Aminoglycan catabolic process	2.99E − 03
GO:0006030	Chitin metabolic process	2.99E − 03
GO:0006032	Chitin catabolic process	2.99E − 03
GO:0031347	Regulation of defense response	2.99E − 03
GO:0046348	Amino sugar catabolic process	2.99E − 03
GO:1901071	Glucosamine-containing compound metabolic process	2.99E − 03
GO:1901072	Glucosamine-containing compound catabolic process	2.99E − 03
GO:0004568	Chitinase activity	2.99E − 03
GO:0016798	Hydrolase activity, acting on glycosyl bonds	3.83E − 03
GO:0006022	Aminoglycan metabolic process	6.30E − 03
GO:0030145	Manganese ion binding	6.30E − 03
GO:0009845	Seed germination	7.15E − 03
GO:0005618	Cell wall	8.49E − 03
GO:0030312	External encapsulating structure	8.49E − 03
GO:0022607	Cellular component assembly	8.49E − 03
GO:0004553	Hydrolase activity, hydrolyzing *O*-glycosyl compounds	9.65E − 03

Table 2
KEGG enrichment for the DAPS ($P \leq 0.01$).

ko-ID	Description	*P*-value
ko00945	Stilbenoid, diarylheptanoid and gingerol biosynthesis	3.88E − 03
ko00941	Flavonoid biosynthesis	6.42E − 03
ko00903	Limonene and pinene degradation	6.56E − 03
ko00940	Phenylpropanoid biosynthesis	8.20E − 03
ko00620	Pyruvate metabolism	1.19E − 02

3.4. Transcriptional analysis of gene expression

We then evaluated the correspondence between protein levels and mRNA abundance via transcriptional analysis of corresponding genes. Several significantly up- or down-accumulated protein species involving pollen exine formation and mitochondria metabolism were selected for qRT-PCR analysis. Almost of these genes expressed significantly higher in the B-line than in the A-line, matching well with their corresponding protein abundance, except for DRL1 and ABCG26 (Fig. 6, Table 3). Both of their protein abundance was significantly higher in the B-line, while the level of mRNA transcription did not significantly differ (Fig. 6, Table 3). This discrepancy suggests that transcript and corresponding protein species abundance not necessarily connected for posttranslational modifications [47].

3.5. ROS contents and antioxides enzyme activity

We measured ROS content (O_2^-, H_2O_2, and MDA) and tested

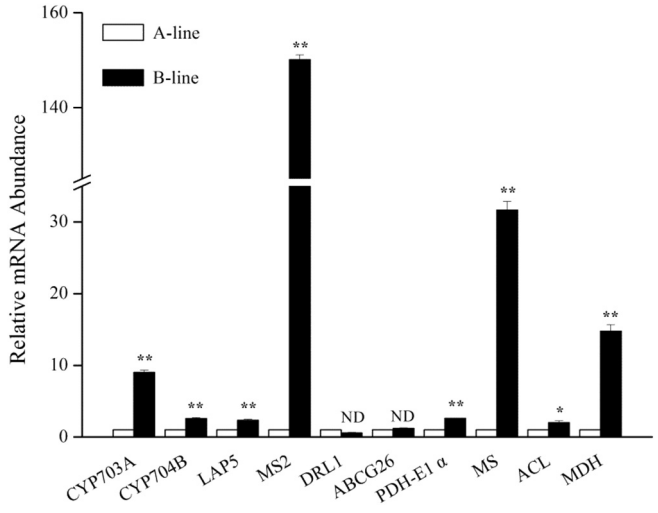

Fig. 6. Relative mRNA abundance of genes encoding proteins related to pollen exine formation and mitochondria metabolism by qRT-PCR. CYP703A, Cytochrome P450 703A; CYP704B, Cytochrome P450 704B; LAP5: Less adhesive pollen 5; MS2: Male sterility 2; DRL1: Dihydroflavonol 4-reductase-like 1; ABCG26: ATP-binding cassette transporter G26; ACL: ATP-citrate lyase; MDH: malate dehydrogenase; MS: malate synthase; PDH-E1α: pyruvate dehydrogenase E1α subunit. "*" and "**" indicate significant differences at $P < 0.05$ and $P < 0.01$, respectively. "ND" means no difference. Means ± SE, n = 3.

antioxidant (SOD, POD, CAT and APX) activities (Fig. 7). O_2^- and H_2O_2 content in the A-line were significantly higher than in the B-line. MDA (a major product of lipid peroxidation) was also significantly higher in the A-line. While, the measurement of antioxidant (SOD, POD and CAT) activities showed that all of them were significantly decreased in A-line than in the B-line.

3.6. ELISA validation

To validate the differently accumulated proteins, activities of four enzymes involved in pyruvate metabolism (pyruvate dehydrogenase, PDH), TCA cycle (malate dehydrogenase, MDH) and PDH-bypass pathways (aldehyde dehydrogenase, ALDH; malate synthase, MS) were assayed using ELISA kits. The activities of these four proteins were significantly higher in B-line than in A-line, which matched well with the protein profiles in label-free analysis (Fig. 8, Table 3). These results indicated that label-free is a reliable method for protein identification and quantification. Additionally, another two enzymes involved in TCA cycle (isocitrate dehydrogenase, IDH; citrate synthase, CS) were also selected for activity measurement. All of the enzyme activities were significantly lower in A-line than in B-line, which also validated the inhibition of mitochondria metabolism.

3.7. Organic acids

We measured the contents of some organic acids including pyruvic acid, citric acid and α-ketoglutarate in stamens of A-line and B-line. The contents of citric acid and α-ketoglutarate were significantly higher in B-line than in A-line, while the content of pyruvic acid was significantly decreased (Fig. 9).

4. Discussion

4.1. Protein species involved in pollen exine formation

Several DAPS involved in pollen exine formation (specifically sporopollenin formation) were identified via GO and KEGG analysis (Table 3), and all were significantly up-accumulated or specifically expressed in the B-line compared with the A-line. In *Arabidopsis*, exine formation is dependent on three major developmental processes: primexine formation, callose wall formation, and sporopollenin synthesis [27]. Primexine and the callose wall act as a scaffold for sporopollenin deposition during the tetrad stage [48].

Major DAPS (significantly up-accumulated or specifically accumulated in the B-line; Table 3) linked to sporopollenin formation included LAP5 (Capana08g002676), involved in forming phenylpropanoid precursors from medium to long-chain (C4-C20) fatty acyl-CoA; CYP703A (Capana10g000622), responsible for lauric acid in-chain hydroxylation; CYP704B (Capana01g002203), catalysis of omega-hydroxylation of long-chain fatty acids; and MS2/FAR2 (Capana03g003125), reduction of fatty acyl-CoA and -ACP to fatty alcohols. During sporopollenin biosynthesis, the TCA cycle produces acetyl-CoA for use as a substrate during lauric acid formation in plastids [27]. Acyl-CoA synthetase 5 (ACOS5) then modifies lauric acids and transfers them to the endoplasmic reticulum (ER). After hydroxylation by CYP703A and CYP704B, the products are CoA-esterified again by ACOS5 like proteins. Finally, downstream MS2 and LAP5 convert the modified lauric acids to sporopollenin precursors. DRL1 (TKPR1/2), tetraketide alpha-pyrone reductase-like proteins may be involved in the biosynthesis of hydroxylated tetraketide compounds that also serve as sporopollenin precursors. Previous research has demonstrated that defects in any part of this pathway will produce abnormal pollen with deficient exine, negatively affecting pollen fertility [28–30].

Sporopollenin-precursor transport is likely conducted by ATP-binding cassette (ABC) transporters, a large and widespread protein superfamily that is important in plant development [49]. Here, we identified an ABC transporter (Capana07g002406) homologous to *Arabidopsis* ABCG26/WBC27 (a protein involved in tapetum-to-microspore sporopollenin monomer transport) and showed that it was only detected in the B-line (Table 3). In rice, *ABCG15* is highly expressed in the tapetum, playing a critical role in cuticle and sporopollenin-precursor transport; *abcg15* mutants exhibit pollen exine deficiency [49]. The lack of ABC transporters in the A-line imply that sporopollenin biosynthesis is probably seriously inhibited or may not even occur under CMS. Taken together, these analyses indicate that pollen abortion in CMS pepper is largely due to abnormal pollen exine formation.

4.2. ROS and tapetal programmed cell death

Tapetum is the innermost layers of the anther surrounding the locule. Tapetum cytoplasm is full of plastids, ribosomes, mitochondria, Golgi bodies, endoplasmic reticulum (ER) and lipid bodies [27]. Because the plastids, ER and lipid bodies are the major organelles for fatty acid synthesis and modification, tapetal cells were thought to play an essential role in lipid biogenesis [46,50]. Many evidences indicate that programmed cell death (PCD) of the tapetum supplies nutrients, metabolites, and sporopollenin precursors for proper microspore development [27,45]. The results of our morphological analysis (see "Pollen morphological features") indicated that premature tapetal PCD leads to pollen abortion. This link is in line with *Arabidopsis* data showing that premature or delayed tapetal PCD affects microspore development, eventually leading to male sterility [27]. The key processes linked with PCD and mitochondria involve the decrease of ATP pool, cytochrome *c* and excess reactive oxygen species (ROS) [51,52].

To clarify whether oxidative stress induced premature tapetum PCD, we measured ROS content (O_2^-, H_2O_2, and MDA) and tested antioxidant (SOD, POD and CAT) activities (Fig. 6). The significantly high levels of O_2^- and H_2O_2 content in the A-line indicated some excess ROS emerged in the A-line. A glycolate oxidase 1 (GOX1) homologous protein (Capana08g000164) was detected. GOX1 is a tetrameric FMN-dependent enzyme which oxidizes the glycolate to glyoxylate and H_2O_2 [53]. It's up-regulation means the increasing of H_2O_2 contents. Plant cells possess an enzymatic and nonenzymatic antioxidants system to cope with ROS. The enzymatic system including antioxidant enzymes like superoxide dismutase (SOD), peroxidase (POD), catalase (CAT), ascorbate peroxidase (APX) and so on. Peroxidases are heme-containing

Table 3
List of main function categories of DAPS related to cytoplasmic male sterility (FC > 2 & P < 0.05).

Accession	Coverage	Peptides	pI	Score	Description	Homologous	A. ave	B. ave	A. vs B. FC	P-value
Pollen exine formation										
Capana08g002676	45.95	15	5.54	1060	LAP5/Chalcone and stilbene synthase family protein	AT4G34850	NA	4.82E + 07	NA	NA
Capana05g000665	32.06	9	6.44	839	DRL1/Dihydroflavonol 4-reductase-like 1	AT4G35420	6.43E + 06	3.96E + 07	1.62E − 01	2.00E − 04
Capana01g002203	43.25	19	6.92	791	CYP704B/Cytochrome P450, family 704, subfamily B	AT1G69500	2.07E + 06	2.04E + 07	1.02E − 01	1.18E − 02
Capana10g000622	5.46	3	7.03	79	CYP703A/Cytochrome P450, family 703, subfamily A	AT1G01280	NA	2.51E + 06	NA	NA
Capana03g003125	11.30	5	8.87	144	MS2,FAR2/Jojoba acyl CoA reductase-related male sterility protein	AT3G11980	NA	4.38E + 06	NA	NA
Capana07g002406	8.77	5	8.84	87	ABCG26,WBC27/ATP-binding cassette transporter G26	AT3G13220	NA	4.52E + 06	NA	NA
Tricarboxylic acid cycle										
Capana01g003447	56.63	13	7.43	2070	MDH/Malate dehydrogenase family protein	AT5G43330	2.69E + 06	1.44E + 07	1.87E − 01	4.30E − 03
mtETC/ATP										
Capana02g003455	30.30	14	8.03	404	NADH-CoQ/NADH dehydrogenase activity	AT5G08530	7.90E + 06	3.77E + 07	2.10E − 01	4.56E − 03
Capana11g002222	6.63	2	6.89	89	COX1/Cytochrome-c oxidase activity	ATMG01360	NA	6.52E + 06	NA	NA
Capana11g000598	19.20	7	6.07	457	ATPQ/Hydrogen ion transmembrane transporter activity	AT3G52300	7.45E + 06	1.54E + 07	4.85E − 01	1.91E − 02
Glycolysis										
Capana04g000900	56.69	25	6.14	2664	PGM3/Phosphoglucomutase 3	AT1G23190	5.27E + 06	2.71E + 07	1.95E − 01	2.16E − 02
Capana01g000823	10.32	4	7.09	80	PKP3/Pyruvate kinase activity	AT1G32440	NA	1.30E + 06	NA	NA
Capana03g002084	24.05	10	7.34	574	PKP1/Pyruvate kinase activity	AT5G52920	5.17E + 06	1.88E + 07	2.75E − 01	1.84E − 04
Capana10g001920	48.20	19	6.73	1623	Pyruvate kinase activity	AT3G52990	1.06E + 07	4.29E + 07	2.47E − 01	6.03E − 04
Capana01g002077	7.27	2	6.65	186	Pyruvate kinase activity	AT5G56350	1.33E + 06	5.76E + 06	2.32E − 01	2.48E − 02
Capana05g000670	28.82	13	7.53	580	Pyruvate kinase activity	AT5G63680	1.51E + 06	1.26E + 07	1.19E − 01	4.06E − 02
Acetyl-CoA biosynthetic process										
Capana09g000016	14.64	6	6.42	484	PDH-E1α/Pyruvate dehydrogenase (acetyl-transferring) activity	AT1G01090	9.46E + 06	2.16E + 07	4.38E − 01	3.01E − 03
Capana11g001244	14.66	6	6.04	345	ACL/ATP-citrate lyase A-2	AT1G60810	2.86E + 06	5.84E + 06	4.89E − 01	6.79E − 03
ALDH										
Capana03g000987	55.07	22	8.25	6188	ALDH2A/Aldehyde dehydrogenase (NAD) activity	AT3G48000	4.18E + 07	2.39E + 08	1.75E − 01	4.69E − 06
Capana11g001334	48.17	16	7.90	6124	ALDH2B/Aldehyde dehydrogenase (NAD) activity	AT1G23800	8.80E + 07	5.12E + 08	1.72E − 01	3.25E − 05
Capana09g000318	4.04	2	6.39	179	ALDH1A/Aldehyde dehydrogenase (NAD) activity	AT3G24503	1.40E + 06	8.24E + 06	1.70E − 01	5.33E − 03
Capana11g001333	52.49	9	9.09	3885	ALDH2B/Aldehyde dehydrogenase (NAD) activity	AT1G23800	3.69E + 07	3.33E + 08	1.11E − 01	1.11E − 05
Glyoxylate cycle										
Capana03g001354	21.72	11	7.78	136	MS/Malate synthase activity	AT5G03860	NA	9.42E + 06	NA	NA
Response to oxidative stress										
Capana00g002177	7.40	2	5.14	170	PRX52/Response to oxidative stress	AT5G05340	5.77E + 06	NA	NA	NA
Capana02g002748	24.32	5	8.38	154	PRX72/Response to oxidative stress	AT5G66390	2.91E + 06	NA	NA	NA
Capana12g000410	32.23	5	5.5	116	PRX/Response to oxidative stress	AT2G24800	3.50E + 06	NA	NA	NA
RNA modification										
Capana03g002028	14.17	3	5.69	172	ATO/RNA binding	AT5G06160	4.12E + 06	1.36E + 06	3.02E + 00	2.28E − 02
Capana01g001807	5.22	2	5.25	67	UBA2A/Nucleic acid binding	AT3G56860	1.56E + 06	3.64E + 06	4.29E − 01	1.32E − 02
Capana05g000453	9.10	5	5	262	CDC5/RNA splicing	AT1G09770	2.48E + 06	5.82E + 06	4.26E − 01	5.93E − 03
Capana12g000228	3.52	3	6.65	211	RCF1/RNA splicing	AT1G20920	3.70E + 06	1.04E + 07	3.56E − 01	5.87E − 03
Capana06g001468	10.18	4	5.44	130	UAP56A/RNA splicing	AT5G11170	1.88E + 06	6.41E + 06	2.94E − 01	7.72E − 03
Capana00g003324	19.93	3	8.97	315	Nucleic acid/nucleotide binding protein	AT1G21320	9.69E + 06	1.98E + 07	4.90E − 01	2.89E − 02
Capana03g001701	26.90	23	6.1	831	ACD/Alanyl-tRNA synthetase	AT1G50200	2.00E + 07	6.75E + 06	2.97E + 00	3.31E − 03
Capana08g001631	9.98	4	8.41	52	NOP56/rRNA modification	AT1G56110	1.15E + 06	NA	NA	NA
Protein modification process										
Capana03g000025	16.33	9	6.68	627	MNS1/Protein glycosylation	AT1G51590	1.03E + 07	3.94E + 06	2.62E + 00	2.62E − 02
Capana02g001484	9.24	4	7.21	53	MNS3/Protein glycosylation	AT1G30000	1.71E + 06	3.11E + 05	5.49E + 00	1.35E − 02
Capana00g002216	3.54	3	8.57	54	PARP1/DNA ligation involved in DNA repair	AT2G31320	NA	1.37E + 06	NA	NA
Capana01g001120	18.10	2	8.31	93	DAD1/Protein *N*-linked glycosylation	AT1G32210	8.59E + 06	1.95E + 07	4.40E − 01	3.60E − 02
Capana12g002139	5.70	2	5.78	58	CPK1/Calcium-dependent protein kinase activity	AT5G04870	2.91E + 06	NA	NA	NA
Capana02g001038	7.00	3	6.00	101	methyltransferase activity	AT5G14260	NA	2.84E + 06	NA	NA

(continued on next page)

Table 3 *(continued)*

Accession	Coverage	Peptides	pI	Score	Description	Homologous	A. ave	B. ave	A. vs B. FC	*P*-value
Capana05g000544	19.11	6	8.46	230	GSTL2/Protein glutathionylation	AT3G55040	6.87E + 06	3.34E + 06	2.06E + 00	1.73E − 02
Capana08g002008	11.67	2	6.60	193	CP24/Light harvesting complex of photosystem II	AT1G15820	1.23E + 07	3.82E + 07	3.23E − 01	1.77E − 02
Capana07g002244	17.23	12	5.15	630	UBP14/Protein deubiquitination	AT3G20630	3.35E + 06	8.48E + 06	3.95E − 01	7.28E − 05
Capana06g000799	26.29	4	5.21	61	UBC27/Protein polyubiquitination	AT5G50870	2.40E + 06	8.55E + 06	2.81E − 01	3.65E − 02
Proteasome-mediated ubiquitin-dependent protein catabolic process										
Capana10g000335	6.93	4	5.08	69	RPN1A/Encoding the RPN subunits of the 26S proteasome	AT2G20580	NA	1.18E + 06	NA	NA
Capana02g000567	22.25	8	4.86	1290	RAD23/Proteasome-mediated ubiquitin-dependent protein catabolic	AT1G79650	4.13E + 07	1.91E + 07	2.17E + 00	1.54E − 02
Capana05g002249	6.48	2	5.68	48	Proteasome component (PCI) domain protein	AT4G19006	1.78E + 06	NA	NA	NA
Tyrosine metabolism and isoquinoline alkaloid biosynthesis										
Capana09g001054	5.14	2	6.48	46	TYRDC1/t-tyrosine decarboxylase	AT4G28680	2.96E + 06	NA	NA	NA
Capana02g003208	18.45	12	7.42	1111	PPO/Polyphenol oxidase	AAA85122	1.36E + 07	5.59E + 06	2.44E + 00	3.09E − 05
Capana01g001179	43.66	22	6.62	6248	CO/Catechol oxidase	XP_016573822	2.85E + 08	1.42E + 08	2.01E + 00	2.29E − 02
Phenylpropanoid biosynthesis										
Capana11g000505	6.39	2	7.21	47	Agmatine coumaroyltransferase-2-like isoform	XP_006340285	1.04E + 06	NA	NA	NA
Capana03g001732	22.61	4	5.27	65	4CL3/4-coumarate:CoA ligase 3	AT1G65060	2.45E + 06	1.13E + 06	2.18E + 00	1.18E − 02

proteins oxidizing various substrates using hydrogen peroxide as electron donor [54]. In the present research, three members of peroxidase superfamily proteins were identified and all of them were specifically expressed in A-line (Table 3). These evidences indicated that some ROS stress emerged in A-line. While, the measurement of antioxidant (SOD, POD and CAT) activities showed that all of them were significantly decreased in A-line than in the B-line (Fig. 7). At the meantime, MDA (a major product of lipid peroxidation) was also significantly higher in the A-line. This increased abundance of oxidative-stress-response proteins with low enzyme activity, and significantly increased MDA contents suggested that the presence of chronic oxidative stress overwhelmed the antioxidant capacity and disrupted the cellular redox balance [31]. We concluded that oxidative stress from excessive ROS probably induced intermediate signals that activated premature tapetum PCD.

4.3. Proteins involved in mitochondria metabolism

As the powerhouses of the cell, mitochondria are not only the center of oxygen consumption but also one of the sources of cellular reactive oxygen species (ROS) [55,56]. DAPS involved in mitochondria metabolism support a link between mitochondrial function and CMS. As a center of energy metabolism, the defects in mitochondria will inevitably affect metabolic process like the TCA cycle, respiratory electron transfer, ATP synthesis [33,57], and further affect the development of reproductive organs and male sterility [14,58].

4.3.1. DAPS involved in TCA cycle

We identified a key protein species associated with the TCA cycle in mitochondria, malate dehydrogenase (MDH), and found its abundance was significantly lower in the A-line than in the B-line (Table 3, Fig. 8). Additionally, the mRNA levels of these protein species and enzyme activity confirmed the corresponding protein abundance (Fig. 6). These results indicated that the TCA cycle was inhibited under CMS and the down regulation of another two TCA cycle involving enzymes (IDH and CS) validated this hypothesis. Similarly, the down-regulation of TCA-cycle enzymes in Honglian rice [59] and wheat [31] causes male sterility.

The TCA cycle also plays an essential role in carbohydrates metabolism. Thus, its inhibition is highly likely to be a primary CMS mechanism. Primary metabolite analysis in pummelo, for example, indicated that carbohydrate metabolism in mitochondria differed between the fertile HBP line and the male sterile hybrid line (G1 + HBP) [1]. Specifically, HBP accumulated more sugar and organic acids than G1 + HBP during the early stage of floral bud development, allowing proper anther and pollen production. In this study, the lower concentrations of citric acid and α-ketoglutarate in stamens of A-line further validate the inhibition of TCA cycle and also suggested that TCA cycle directly or indirectly affected the sterility of stamens in pepper (Fig. 9).

4.3.2. DAPS involved in electron transport chain (mtETC) and ATP synthesis

Furthermore, the mitochondrial electron transport chain (mtETC) and ATP synthesis were very likely to be inhibited under CMS, as the TCA cycle provides NADH and $FADH_2$ to mtETC. In support of this, DAPS related to mtETC/ATP synthesis were selected for further analysis (Table 3). NADH dehydrogenase (NADH-CoQ) (also referred to complex I), is the first enzyme of the mitochondrial electron transport chain, catalyzing the transfer of electrons from NADH to subsequent complexes. The down regulation of NADH dehydrogenase (ubiquinone) (Capana02g003455) suggested a limitation of the electron transport. Furthermore, the D-subunit of ATP synthase, ATPQ (Capana11g000598), was identified. Mitochondrial membrane ATP synthase (F1F0 ATP synthase or Complex V) produces ATP from ADP in the presence of a proton gradient which is generated by electron transport chain [60]. Its less accumulation suggested a reducing ATP production

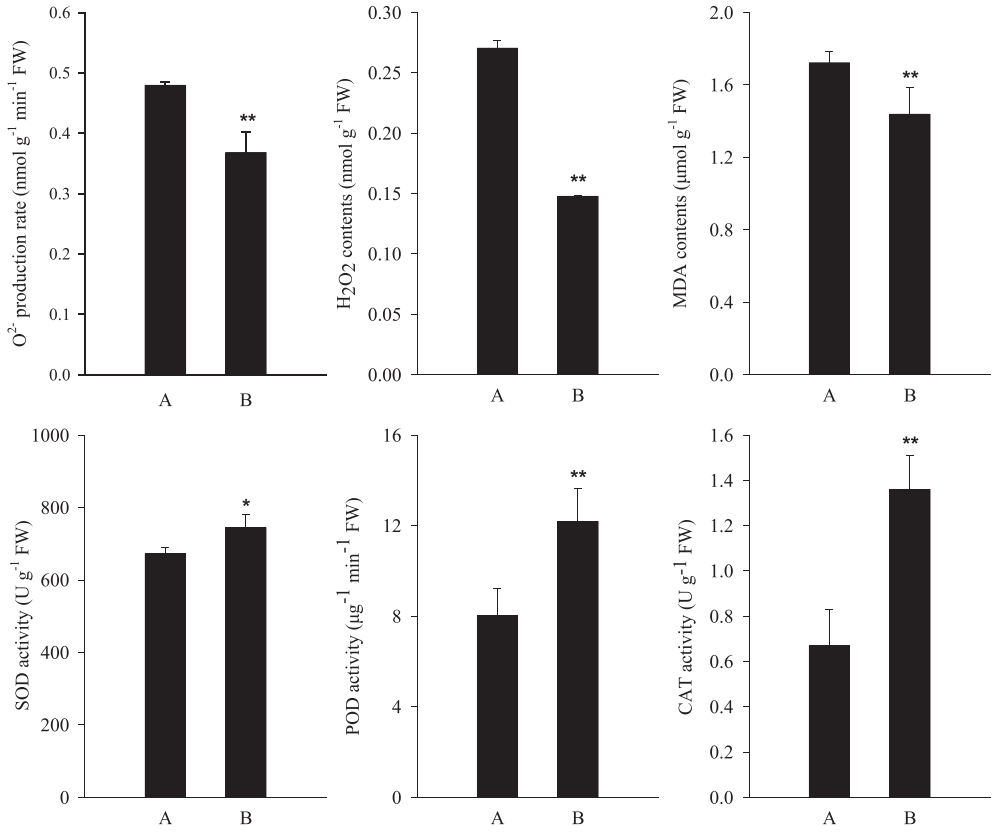

Fig. 7. Reactive oxygen species (ROS) content and antioxidant enzyme activity. "A" indicate A-line; "B" indicate B-line. "*" and "**" indicate significant difference at $P < 0.05$ and $P < 0.01$, respectively. Means ± SE, n = 3.

and low energy output. As the result, the reduced ATP pool and excessive ROS generated by slowing down of electron transfer, disturbed the redox homeostasis, and ultimately induced premature tapetum PCD. The production of excessive ROS was validated by the accumulation of O_2^-, H_2O_2, MDA and the activities of antioxidant enzymes above (Fig. 7).

4.3.3. DAPS involved in pyruvate metabolism

We also found evidence for the involvement of the pyruvate dehydrogenase (PDH) complex in pollen development and therefore pollen

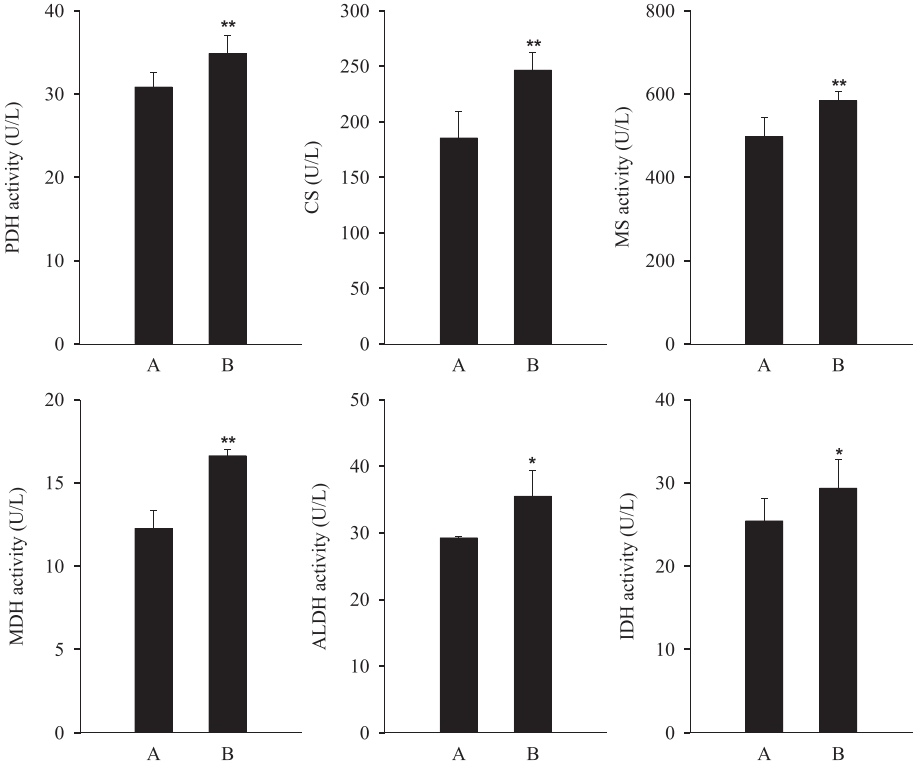

Fig. 8. Enzyme activities assayed by ELISA. "A" indicate A-line; "B" indicate B-line. PDH: pyruvate dehydrogenase; CS: citrate synthase; MS: malate synthase; MDH: malate dehydrogenase; ALDH: aldehyde dehydrogenase; IDH: isocitrate dehydrogenase. "*" and "**" indicate significant differences at $P < 0.05$ and $P < 0.01$, respectively. Means ± SE, n = 3.

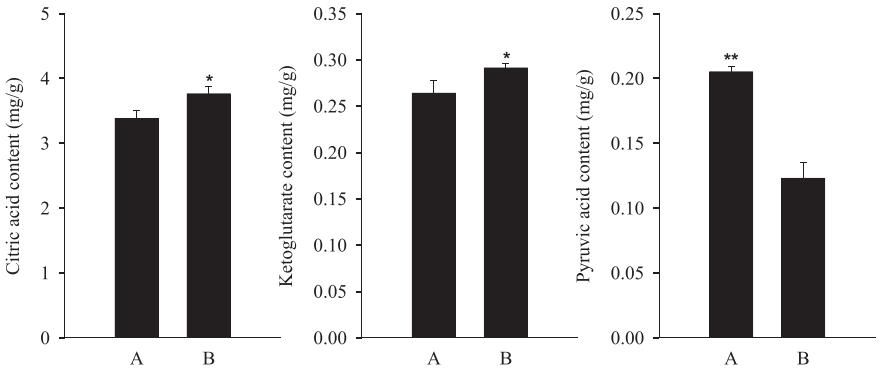

Fig. 9. Contents of organic acids. "A" indicate A-line; "B" indicate B-line. "*" and "**" indicate significant differences at $P < 0.05$ and $P < 0.01$, respectively. Means ± SE, n = 3.

dysfunction. Protein species related to this complex (PDH-E1α homologs) were significantly down-accumulated in A-line (Table 3), suggesting some form of pyruvate metabolism inhibition. The down-regulated enzyme activity of PDH and the increased pyruvic acid contents suggested that the transform process of pyruvate to acetyl-CoA was inhibited. As a center of sucrose metabolism and energy production, the defects in any members of PDH complex will manifest as disorders, ranging from mild to severe disorder [61], including male sterility. For example, PDH-E1α-1 inhibition in sugar beet caused tapetum swelling and abnormal vacuolation, leading to pollen abortion [5]. Additionally, proteomic analysis of Honglian rice anthers indicated that the lack of PDH-E1-β is associated with pollen sterility [62]. These data combined indicate that defects of the PDH complex in pepper likely related to pollen sterility.

Pyruvate links the glycolysis with the TCA cycle, glyconeogenesis and ethanol formation. As we know, pyruvate is a key metabolite in cells which mainly originated from glycolysis by pyruvate kinase. Five pyruvate kinases homologous and a cytosolic phosphoglucomutase (cPGM) were identified in this research (Table 3), and all of them were significantly up-accumulated or specifically detected in B-line. Cytosolic phosphoglucomutase (cPGM, Capana04g000900) is a key enzyme in glycolysis pathway which interconverts glucose 6-phosphate and glucose 1-phosphate. In *Arabidopsis*, loss of both cPGM genes (*PGM2* and *PGM3*) severely impaired male and female gametophyte development [63]. Since the pyruvate dehydrogenase (PDH) complex is an essential and rate-limiting enzyme connecting glycolysis with the TCA cycle [64], the defects of PDH complex may feedback inhibit the glycolysis. The PDH complex produces acetyl-CoA, not only used for TCA cycle, but also used in de novo fatty acid synthesis during pollen exine formation [5]. Additionally, ATP-citrate lyase (ACL) catalyzes the ATP-dependant reaction of citrate and CoA to form acetyl-CoA and oxaloacetic acid. These data suggested that the decrease of PDH complex will decrease the pollen exine formation. And the inhibition event of pollen exine formation has been clarified above.

Moreover, we identified four aldehyde dehydrogenase (ALDH)-related protein species involved in PDH-bypass pathways, and all were highly accumulated in the B-line, but not in the sterile A-line. This pattern suggests that ALDH down-regulation is likely involved in pepper CMS. Interestingly, malate synthase was detected only in the B-line (Table 3), and its relative transcript abundance also significantly higher there (Fig. 6). As this enzyme is important to the glyoxylate cycle, a failure to detect malate synthase indicated that the glyoxylate cycle probably does not occur in the A-line.

These results suggested that PDH-bypass pathways must play a critical role in CMS. The main enzymes in these pathways are pyruvate decarboxylase (PDC), ALDH, and acetyl-CoA synthetase (ACS) [65]. First, PDC produces acetaldehyde from pyruvate. Next, acetaldehyde is either reduced by alcohol dehydrogenase (ADH) or oxidized by ALDH to form acetate, which is then converted to acetyl-CoA. Finally, ACS then acts on acetyl-CoA in the glyoxylate cycle [65]. These pathways probably produce high concentrations of aldehyde and alcohol as toxic by-products during the energy-intensive processes of pollen development. Toxic by-products disrupt ROS homeostasis, thus causing oxidative stress and damaging DNA, proteins, and lipids. Eventually, these conditions trigger premature tapetum cell death. Thus, ALDH probably functions to detoxify plant cells under normal pollen development, and we hypothesized that the disruptions to this process, including ALDH down-regulation or dysfunction, may contribute strongly to CMS. Indeed, the fertility restoration gene *Rf2* in maize actually encodes an aldehyde dehydrogenase [14,62]. In humans, subtle changes to ALDH content and properties are likely to induce ethanol-related diseases [66,67] and this effect may have a parallel in plants.

4.4. DAPs involved in posttranscriptional and posttranslational modification

The discrepancy between the mRNA level and corresponding protein species abundance indicated the absence of posttranscriptional regulation and posttranslational modifications (Fig. 6, Table 3). In this study, several DAPS related to mRNA modification has been detected and showed in Table 3, such as CDC5, a DNA binding protein involving in regulating posttranscriptional processing or transcription of primary miRNA transcripts [68,69]; UAP56 and RCF1, a DEAD box RNA helicase involving in mRNA splicing and export [70,71]. Besides what mentioned above, posttranslational modifications play important roles in modulating various biological functions. Protein degradation is a key posttranslational event that maintains cellular homeostasis, and ubiquitin (Ub)/26S proteasome system (UPS) is a major proteolytic pathway in plants [72]. Protein species involved in proteasome-mediated ubiquitin-dependent protein catabolic process were detected in this study. RAD23 proteins play an essential role in the fertility of plants by delivering UPS (ubiquitin (Ub)/26S proteasome system) substrates to the 26S proteasome [73,74]. RPN1A encoding the RPN subunits of the 26S proteasome. Their significant up or down accumulation in A-line (Table 3) suggested a potential unnormal protein degradation. In this study, the up or down accumulation of protein species involved in posttranscriptional and posttranslational modification process indicated that a complicated mechanism regulating pollen fertility in pepper.

4.5. Up-accumulated proteins in A-line

We performed KEGG analysis to further understand the significantly changed pathways among the up-accumulated proteins in A-line. As a result, we found that DAPs involved in isoquinoline alkaloid biosynthesis, tyrosine metabolism and phenylpropanoid biosynthesis were significantly enriched ($P < 0.05$). And these proteins have been listed in Table 3. Tyrosine is the substrate of isoquinoline alkaloid biosynthesis which begins with the decarboxylation of tyrosine to yield tyramine by tyrosine decarboxylase (TYRDC) [75]. TYRDC is a member of aromatic amino acid decarboxylases (AAADs) which catalyze key reactions impacting the synthase of alkaloids, aromatic volatiles and antioxidant

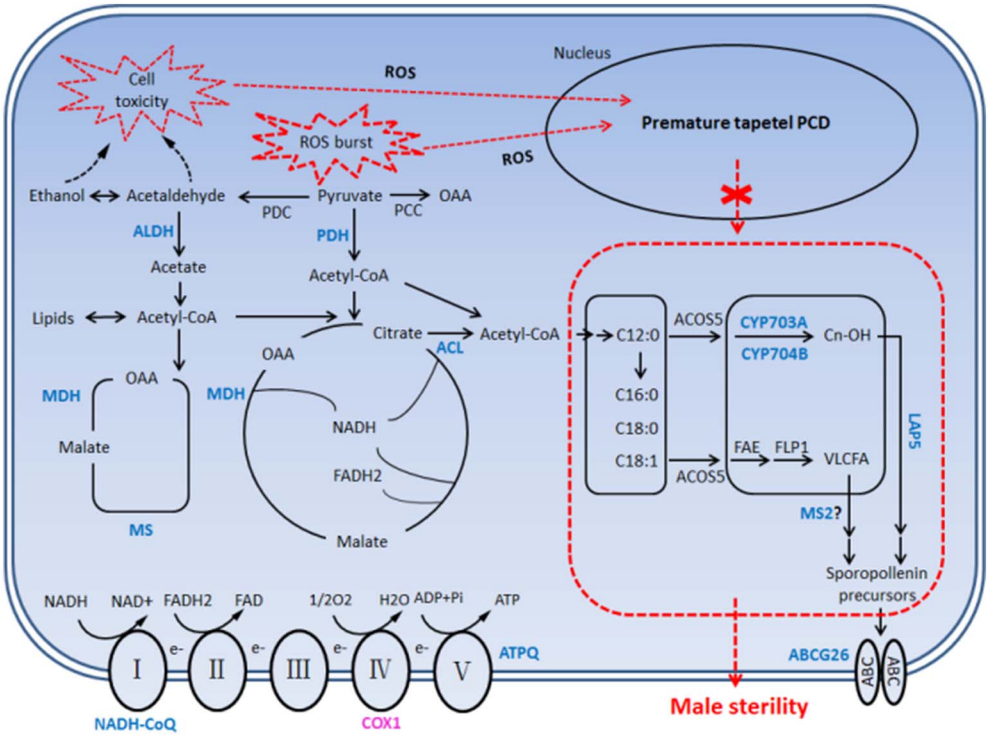

Fig. 10. A protein network for cytoplasmic male sterility. Protein descriptions and abundance are listed in Table 3. "Blue" indicates down-regulation and "magenta" indicates up-regulation in the A-line. ACOS5: Acetyl-CoA synthetase 5; CYP703A: Cytochrome P450 703A; CYP704B: Cytochrome P450 704B; FAE: Fatty acid elongation; FLP1: Faceless pollen-1; DRL1: Dihydroflavonol 4-reductase-like 1; MS2: Male sterility 2; LAP5: Less adhesive pollen 5; ABCG26: ATP-binding cassette transporter G26; PDH: pyruvate dehydrogenase; MDH: malate dehydrogenase; ACL: ATP-citrate lyase; MS: malate synthase; ALDH: aldehyde dehydrogenase; PCC: phosphoenolpyruvate carboxylase; PDC: pyruvate decarboxylase; COX1: cytochrome-*c* oxidase I; ATPQ: ATP synthase subunits.

in plants [76,77]. Phosphoenolpyruvic acid (PEP), the product of glycolysis, may be used for the synthesis of pyruvate to participate in the TCA cycle, or be used for synthesis of chorismate through the shikimate pathway to form the aromatic amino acids like tyrosine. In this study, in increased contents of pyruvic acid may feedback inhibit the transformation of PEP to pyruvic acids. The up-accumulated proteins involved in isoquinoline alkaloid biosynthesis and tyrosine metabolism in A-line indicated that more PEP were involved in shikimate pathway not in TCA cycle, and further illustrated the inhibition of pyruvate metabolism and TCA cycle. Polyphenol oxidases (PPOs) known as catechol oxidases (COs) catalyzing the oxygen-dependent oxidation of phenols to quinones and assumed to be involved in plant defense against abiotic and biotic stress [78]. Phenolic compounds have been demonstrated to relate to disease susceptibility in plants. And the reduction of phenylpropanoid levels can also increase disease susceptibility [79]. The up-accumulation of proteins homologous to PPO, CO or related to phenylpropanoid biosynthesis indicated some degree of oxidative stress induced in the stamens of A-line.

4.6. Proposed CMS model

Based on our results, we now propose a potential protein network for CMS. We suggest that the TCA cycle is likely to be limited by the inhibition of pyruvate metabolism in CMS plants, stopping or greatly decreasing NADH and $FADH_2$ production. In turn, the mtETC and ATP synthesis are also inhibited, which eventually leads to excessive ROS production and oxidative stress. Together, reduced ATP, ROS burst, and cytochrome *c* release [67] cause premature tapetum PCD. Additionally, ALDH down-regulation inhibits the glyoxylate cycle, resulting in excess aldehyde and alcohol that increases cellular toxicity and contributing to the ROS burst. These problems kill off tapetal cells, which then tightly surround tetrad microspores, ultimately causing their rupture and death. Furthermore, sporopollenin biosynthesis and transport are severely inhibited, preventing the formation of exine and leading to pollen abortion.

5. Conclusions

In this study, we identified numerous proteins associated with pollen development and male sterility by label-free analysis. A total of 324 DAPS were identified and quantified. The histological analysis indicated that the premature tapetum PCD may be the main reason of male sterility. Bioinformatics analysis suggested that DAPS involved in pollen exine formation, pyruvate metabolic processes, the tricarboxylic acid cycle, the mitochondrial electron transport chain, and oxidative stress response might be related to pollen abortion in pepper. Based on our results, we proposed a protein network to explain the mechanisms of cytoplasmic male sterility (Fig. 10). Our data and model provide insight into pepper CMS and contribute to the improvement of pepper hybrid breeding.

Supplementary data to this article can be found online at http://dx.doi.org/10.1016/j.jprot.2017.08.013.

Conflicts of interest statement

The authors declare no competing financial interests.

Author contributions

Jinju Guo performed most of the experiments, analyzed the data, and drafted the manuscript. Peng Wang performed the semi-thin paraffin section analysis. Qing Cheng and Limin Sun participated in the measurement of physiological parameters. Hongyu Wang and Yutong Wang performed the qRT-PCR analysis. Lina Kao and Yanan Li assisted with sampling and data analysis. Tuoyu Qiu performed literature searches. Wencai Yang revised the manuscript. Huolin Shen designed and directed the entire study. All authors have read and approved the final manuscript.

Acknowledgments

This work was supported by the National Key Research and Development Program of China (2016YFD0101704) and the Beijing

Fruit Vegetables Innovation Team of Modern Agricultural Industry Technology System (BAIC01-2017).

References

[1] B.B. Zheng, Y.N. Fang, Z.Y. Pan, L. Sun, X.X. Deng, J.W. Grosser, W.W. Guo, iTRAQ-based quantitative proteomics analysis revealed alterations of carbohydrate metabolism pathways and mitochondrial proteins in a male sterile cybridpummelo, J. Proteome Res. 13 (2014) 2998–3015.
[2] P.S. Schnable, P.R. Wise, The molecular basis of cytoplasmic male sterility and fertility restoration, Trends Plant Sci. 3 (1998) 175–180.
[3] C.A. Makaroff, I.J. Apel, J.D. Palmer, The role of coxI-associated repeated sequences in plant mitochondrial DNA rearrangements and radish cytoplasmic male sterility, Curr. Genet. 19 (1991) 183–190.
[4] P. Bergman, J. Edqvist, I. Farbos, K. Glimelius, Malesterile tobacco displays abnormal mitochondrial atp1 transcript accumulation and reduced floral ATP/ADP ratio, Plant Mol. Biol. 42 (2000) 531–544.
[5] R. Yui, S. Iketani, T. Mikami, T. Kubo, Antisense inhibition of mitochondrial pyruvate dehydrogenase E1α subunit in anther tapetum causes male sterility, Plant J. 34 (2003) 57–66.
[6] S. He, A. Lyznik, S. Mackenzie, Pollen fertility restoration by nuclear gene Fr in CMS bean: nuclear-directed alteration of a mitochondrial population, Genetics 139 (1995) 955–962.
[7] C.D. Chase, Cytoplasmic male sterility: a window to the world of plant mitochondrial-nuclear interactions, Trends Gent. 23 (2007) 81–90.
[8] N. Glab, R.P. Wise, D.R. Pring, C. Jacq, P. Slonimski, Expression in *Saccharomyces cerevisiae* of a gene associated with cytoplasmic male sterility from maize: respiratory dysfunction and uncoupling of yeast mitochondria, Mol Gen Genet 223 (1990) 24–32.
[9] L.M. Prioli, J.T. Huang, C.S. Levings III, The plant mitochondrial open reading frame *orf221* encodes a membranebound protein, Plant Mol. Biol. 23 (1993) 287–295.
[10] J.L. Heazlewood, J. Whelan, A.H. Millar, The products of the mitochondrial *orf25* and *orfB* genes are F_o components in the plant F_1F_o ATP synthase, FEBS Lett. 540 (2003) 201–205.
[11] R.P. Wise, A.E. Fliss, D.R. Pring, B.G. Gengenbach, *urf13-T* of T cytoplasm maize mitochondria encodes a 13 kD polypeptide, Plant Mol. Biol. 9 (1987) 121–126.
[12] M.L. Boeshore, M.R. Hanson, S. Izhar, A variant mitochondrial DNA arrangement specific to petunia stable sterile comatic hybrids, Plant Mol. Biol. 4 (1985) 125–132.
[13] E.G. Young, M.R. Hanson, A fused mitochondrial gene associated with cytoplasmic male sterility is developmentally regulated, Cell 50 (1987) 41–49.
[14] M.R. Hanson, S. Bentolila, Interactions of mitochondrial and nuclear genes that affect male gametophyte development, Plant Cell 16 (2004) 154–169.
[15] J.S. Song, C. Hedgcoth, A chimeric gene (*orf256*) is expressed as protein only in cytoplasmic male-sterile lines of wheat, Plant Mol. Biol. 26 (1994) 535–539.
[16] R. Horn, R.H. Köhler, K. Zetsche, A mitochondrial 16 kDa protein is associated with cytoplasmic male sterility in sunflower, Plant Mol. Biol. 17 (1991) 29–36.
[17] F. Monéger, C.J. Smart, C.J. Leaver, Nuclear restoration of cytoplasmic male sterility in sunflower is associated with the tissue specific regulation of a novel mitochondrial gene, EMBO J. 13 (1994) 8–17.
[18] M. Sabar, D. Gagliardi, J. Balk, C.J. Leaver, ORFB is a subunit of F_1F_O-ATP synthase: insight into the basis of cytoplasmic male sterility in sunflower, EMBO Rep. 4 (2003) 1–6.
[19] M. Hernould, S. Suharsono, S. Litvak, A. Araya, A. Mouras, Male sterility induction in transgenic tobacco plants with an unedited *apt*9 mitochondrial gene from wheat, Proc. Natl. Acad. Sci. U. S. A. 90 (1993) 2370–2374.
[20] B. Jing, S.P. Heng, D. Tong, Z.J. Wan, T.D. Fu, J.X. Tu, C.Z. Ma, B. Yi, J. Wen, J.X. Shen, A male sterility-associated cytotoxic protein ORF288 in *Brassica juncea* causes aborted pollen development, J. Exp. Bot. 63 (2012) 1285–1295.
[21] P. Kumar, N. Vasupalli, R. Srinivasan, S.R. Bhat, An evolutionarily conserved mitochondrial *orf108* is associated with cytoplasmic male sterility in different alloplasmic lines of *Brassica juncea* and induces male sterility in transgenic *Arabidopsis thaliana*, J. Exp. Bot. 63 (2012) 2921–2932.
[22] H.W. Tang, D.P. Luo, D.G. Zhou, Q.Y. Zhang, D.S. Tian, X.M. Zheng, L.T. Chen, Y.G. Liu, The rice restorer *Rf4* for wild-abortive cytoplasmic male sterility encodes a mitochondrial-localized PPR protein that functions in reduction of *WA352* transcripts, Mol. Plant 7 (2014) 1497–1500.
[23] D.P. Luo, H. Xu, Z.L. Liu, J.X. Guo, H.Y. Li, L.T. Chen, C. Fand, Q.Y. Zhang, M. Bai, N. Yao, Hong Wu, Hao Wu, C.H. Ji, Y.L. Chen, S. Ye, X.Y. Li, X.C. Zhao, R.Q. Li, Y.G. Liu, A detrimental mitochondrial-nuclear interaction causes cytoplasmic male sterility in rice, Nat. Genet. 45 (2013) 573–577.
[24] F. Ahlers, I. Thoma, J. Lambert, R. Kuckuk, R. Wiermann, ^{1}H NMR analysis of sporopollenin from *Typha Angustifolia*, Phytochemistry 50 (1999) 1095–1098.
[25] F. Ahlers, H. Bubert, S. Steuernagel, R. Wiermann, The nature of oxygen in sporopollenin from the pollen of *Typha angustifolia* L. Z. Naturforsch. C 55 (2000) 129–136.
[26] A.A. Dobritsa, A. Geanconteri, J. Shrestha, A. Carlson, N. Kooyers, D. Coerper, E. Urbanczyk-Wochniak, B.J. Bench, L.W. Sumner, R. Swanson, D. Preuss, A large-scale genetic screen in *Arabidopsis* to identify genes involved in pollen exine production, Plant Physiol. 157 (2011) 947–970.
[27] T. Ariizumi, K. Toriyama, Pollen exine pattern formation is dependent on three major developmental processes in *Arabidopsis thaliana*, Annu. Rev. Plant Biol. 62 (2007) 437–460.
[28] A.A. Dobritsa, J. Shrestha, M. Morant, F. Pinot, M. Matsuno, R. Swanson, B.L. Møller, D. Preuss, CYP704B1 is a long-chain fatty acid omega-hydroxylase essential for sporopollenin synthesis in pollen of *Arabidopsis*, Plant Physiol. 151 (2009) 574–589.
[29] H. Li, F. Pinot, V. Sauveplane, D. Werck-Reichhart, P. Diehl, L. Schreiber, R. Franke, P. Zhang, L. Chen, Y.W. Gao, W.Q. Liang, D.B. Zhang, Cytochrome P450 family member CYP704B2 catalyzes the ω-hydroxylation of fatty acids and is required for anther cutin biosynthesis and pollen exine formation in rice, Plant Cell 22 (2010) 173–190.
[30] A.A. Dobritsa, Z. Lei, S. Nishikawa, E. Urbanczyk-Wochniak, D.V. Huhman, D. Preuss, LAP5 and LAP6 encode anther-specific proteins with similarity to chalcone synthase essential for pollen exine development in *Arabidopsis*, Plant Physiol. 153 (2010) 937–955.
[31] S.P. Wang, G.S. Zhang, Y.X. Zhang, Q.L. Song, Z. Chen, J.S. Wang, J.L. Guo, N. Niu, J.W. Wang, S.C. Ma, Comparative studies of mitochondrial proteomics reveal an intimate protein network of male sterility in wheat (*Triticumaestivum* L.), J. Exp. Bot. 66 (2015) 6191–6203.
[32] S.Q. Li, C.X. Wan, J. Kong, Z.J. Zhang, Y.S. Li, Y.G. Zhu, Programmed cell death during microgenesis in a Honglian CMS line of rice is correlated with oxidatice stress in mitochondria, Funct. Plant Biol. 31 (2004) 369–376.
[33] Z.M. Wu, J.W. Cheng, C. Qin, Z.Q. Hu, C.X. Yin, K.L. Hu, Differential proteomic analysis of anthers between cytoplasmic male sterile and maintainer lines in *capsicum annuum* L. Int. J. Mol. Sci. 14 (2013) 22982–22996.
[34] B.F.N.M. Ghochani, K. Gilany, Proteomics a key tool for a better understanding of endometriosis: a mini-review, J. Paramed. Sci. 2 (2011) 51–58.
[35] J. Liu, C.Y. Pang, H.L. Wei, M.Z. Song, Y.Y. Meng, J.H. Ma, S. Fan, iTRAQ-facilitated proteomic profiling of anthers from a photosensitive male sterility mutant and wild-type cotton (*Gossypium hirsutum* L.), J. Proteome 126 (2015) 68–81.
[36] E. Gokce, C.M. Shuford, W.L. Franck, R.A. Dean, D.C. Muddiman, Evaluation of normalization methods on geLC-MS/MS label-free spectral counting data to correct for variation during proteomic workflows, J. Am. Soc. Mass Spectrom. 22 (2011) 2199–2208.
[37] J.G. Burniston, J. Connolly, H. Kainulainen, S.L. Britton, L.G. Koch, Label-free profiling of skeletal muscle using high-definition mass spectrometry, Proteomics 14 (2014) 2339–2344.
[38] E.F. Elstner, A. Heupel, Inhibition of nitrite formation from hydroxylammoniumchloride: a simple assay for superoxide dismutase, Anal. Biochem. 70 (1976) 616–620.
[39] C. Gay, J.M. Gebicki, A critical evaluation of the effect of sorbitol on the ferric-xylenol orange hydroperoxide assay, Anal. Biochem. 284 (2000) 217–220.
[40] I. Cakmak, W.J. Horst, Effect of aluminum on lipid peroxidation, superoxide dismutase, catalase, and peroxidase activities in root tips of soybean (Glycine max), Physiol. Plant. 83 (1991) 463–468.
[41] C.N. Giannopolitis, S.K. Ries, Superoxide dismutase: occurrence in high plants, Plant Physiol. 59 (1977) 309–314.
[42] X. Zheng, R.B. Huystee, Peroxidase-regulated elongation of segments from peanuts hypocotyls, Plant Sci. 81 (1992) 47–56.
[43] H. Aebi, Catalase in vitro, Methods Enzymol. 105 (1984) 121–126.
[44] T.D. Quilichini, E. Grienenberger, C.J. Douglas, The biosynthesis, composition and assembly of the outer pollen wall: a tough case to crack, Phytochemistry 113 (2015) 170–182.
[45] P. Piffanelli, J.H.E. Ross, D.J. Murphy, Biogenesis and function of the lipidic structures of pollen grains, Plant Reprod. 11 (1998) 65–80.
[46] I. Hernández-Pinzón, J.H. Ross, K.A. Barnes, A.P. Damant, D.J. Murphy, Composition and role of tapetal lipid bodies in the biogenesis of the pollen coat of *Brassica napus*, Planta 208 (1999) 588–598.
[47] B. Pradet-Balade, F. Boulme, H. Beug, E.W. Mullner, J.A. Garcia-Sanz, Translation control: bridging the gap between genomics and proteomics? Trends Biochem. Sci. 26 (2001) 225–229.
[48] S.Y. Rhee, C.R. Somerville, Tetrad pollen formation in quartet mutants of *Arabidopsis thaliana* is associated with persistence of pectic polysaccharides of the pollen mother cell wall, Plant J. 15 (1998) 79–88.
[49] P. Qin, B. Tu, Y.P. Wang, L.C. Deng, T.D. Quilichini, T. Li, H. Wang, B.T. Ma, S.G. Li, *ABCG15* encodes an ABC transporter protein, and is essential for Post-Meiotic anther and pollen exine development in rice, Plant Cell Physiol. 54 (2013) 138–154.
[50] Y.X. Yang, C.H. Dong, J.Y. Yu, L. Shi, C.B. Tong, Z.B. Li, J.Y. Huang, S.Y. Liu, Cysteine Protease 51 (CP51), an anther-specific cysteine protease gene, is essential for pollen exine formation in *Arabidopsis*, Plant Cell Tissue Org. Cult. 119 (2014) 383–397.
[51] D.R. Green, J.C. Reed, Mitochondria and apoptosis, Science 281 (1998) 1309–1312.
[52] B.S. Tiwari, B. Belenghi, A. Levine, Oxidative stress increased respiration and generation of reactive oxygen species, resulting in ATP depletion, opening of mitochondrial permeability transition, and programmed cell death, Plant Physiol. 128 (2002) (2002) 1271–1281.
[53] P. Kerchev, C. Waszczak, A. Lewandowska, P. Willems, A. Shapiguzov, Z. Li, S. Alseekh, P. Mühlenbock, F.A. Hoeberichts, J.J. Huang, K.V.D. Kelen, J. Kangasjärvi, A.R. Fernie, R.D. Smet, Y.V. de Peer, J. Messens, F.V. Breusegem, Lack of GLYCOLATE OXIDASE1, but not GLYCOLATE OXIDASE2, attenuates the photorespiratory phenotype of CATALASE2-deficient *Arabidopsis*, Plant Physiol. 171 (2016) 1704–1719.
[54] F. Fernández-Péreza, F. Pomarb, M.A. Pedreñoa, E. Novo-Uzala, Suppression of *Arabidopsis* peroxidase 72 alters cell wall and phenylpropanoid metabolism, Plant Sci. 239 (2015) 192–199.
[55] I.M. Møller, A. Rogowska-Wrzesinska, R.S. Rao, Protein carbonylation and metal-catalyzed protein oxidation in a cellular perspective, J. Proteome 74 (2011) 2228–2242.
[56] F. Salvato, J.F. Havelund, M.J. Chen, R. Shyama Prasad Rao, A. Rogowska-

Wrzesinska, O.N. Jensen, D.R. Gang, J.J. Thelen, I.M. Møller, The potato tuber mitochondrial proteome, Plant Physiol. 164 (2014) 637–653.
[57] D.C. Logan, The mitochondrial compartment, J. Exp. Bot. 57 (2006) 1225–1243.
[58] J. Carlsson, M. Leino, J. Sohlberg, J.F. Sundstroem, K. Glimelius, Mitochondrial regulation of flower development, Mitochondrion 8 (2008) 74–86.
[59] Q.P. Sun, C.F. Hu, J. Hu, S.Q. Li, Y.G. Zhu, Quantitative proteomic analysis of CMS-related changes in Honglian CMS rice anther, Protein J. 28 (2009) 341–348.
[60] W. Kühlbrandt, Structure and function of mitochondrial membrane protein complexes, BMC Biol. 13 (2015) 89.
[61] T.L. Huh, J.P. Casazza, J.W. Huh, Y.T. Chi, B.J. Songs, Characterization of two cDNA clones for pyruvate dehydrogenase E1β subunit and its regulation in tricarboxylic acid cycle-deficient fibroblast, J. Biol. Chem. 256 (1990) 13320–13326.
[62] L. Wen, G. Liu, S.H. Li, C.X. Wan, J. Tao, K.Y. Xu, Z.J. Zhang, Y.G. Zhu, Proteomic analysis of anthers from Honglian cytoplasmic male sterility line rice and its corresponding maintainer and hybrid, Bot. Stud. 48 (2007) 293–309.
[63] B. Egli, K. Kölling, C. Köhler, S.C. Zeeman, S. Streb, Loss of cytosolic phosphoglucomutase compromises gametophyte development in *Arabidopsis*, Plant Physiol. 154 (2010) 1659–1671.
[64] H.H.M. Dahl, Pyruvate dehydrogenase E1a deficiency: males and females differ yet again, Am. J. Hum. Genet. 56 (1995) 553–557.
[65] S. Mellema, W. Eichenberger, A. Rawyler, M. Suter, M. Tadege, C. Kuhlemeier, The ethanolic fermentation pathway supports respiration and lipid biosynthesis in tobacco pollen, Plant J. 30 (2002) 329–336.
[66] R. Lindahl, Aldehyde dehydrogenases and their role in carcinogenesis, Crit. Rev. Biochem. Mol. Biol. 27 (1992) 283–335.
[67] R.G.L. op den Camp, C. Kuhlemeier, Aldehyde dehydrogenase in tobacco pollen, Plant Mol. Biol. 35 (1997) 355–365.
[68] C.G. Burns, R. Ohi, A.R. Krainer, K.L. Gould, Evidence that Myb-related CDC5 proteins are required for pre-mRNA splicing, Proc. Natl. Acad. Sci. U. S. A. 96 (1999) 13789–13794.
[69] S.X. Zhang, M. Xie, G.D. Ren, B. Yu, CDC5, a DNA binding protein, positively regulates posttranscriptional processing and/or transcription of primary microRNA transcripts, Proc. Natl. Acad. Sci. U. S. A. 110 (2013) 17588–17593.
[70] C. Kammel, M. Thomaier, B.B. Sørensen, T. Schubert, G. Längst, M. Grasser, K.D. Grasser, *Arabidopsis* DEAD-box RNA helicase UAP56 interacts with both RNA and DNA as well as with mRNA export factors, PLoS One 8 (2013) e60644.
[71] Q. Guan, J. Wu, Y. Zhang, C. Jiang, R. Liu, C. Chai, J. Zhu, A DEAD box RNA helicase is critical for pre-mRNA splicing, cold-responsive gene regulation, and cold tolerance in *Arabidopsis*, Plant Cell 25 (2013) 342–356.
[72] J. Smalle, R.D. Vierstra, The ubiquitin 26S proteasome proteolytic pathway, Annu. Rev. Plant Biol. 55 (2004) 555–590.
[73] A. Ramadan, K. Nemoto, M. Seki, K. Shinozaki, H. Takeda, H. Takahashi, T. Sawasaki, Wheat germ-based protein libraries for the functional characterisation of the *Arabidopsis* E2 ubiquitin conjugating enzymes and the RING-type E3 ubiquitin ligase enzymes, BMC Plant Biol. 15 (2015) 275.
[74] L.M. Farmer, A.J. Book, K.H. Lee, Y.L. Lin, H.Y. Fu, R.D. Vierstraa, The RAD23 family provides an essential connection between the 26S proteasome and ubiquitylated proteins in *Arabidopsis*, Plant Cell 22 (2010) 124–142.
[75] P.J. Facchini, V. De Luca, Opium poppy and Madagascar periwinkle: model non-model systems to investigate alkaloid biosynthesis in plants, Plant J. 54 (2008) 763–784.
[76] E. Leete, S. Kirkwood, L. Marion, The biogenesis of alkaloids: VI. The formation of hordenine and *N*-methyltyramine from tyrosine in barley, Can. J. Chem. 30 (1952) 749–760.
[77] P.J. Facchini, K.L. Huber-Allanach, L.W. Tari, Plant aromatic L-amino acid decarboxylases: evolution, biochemistry, regulation, and metabolic engineering applications, Phytochemistry 54 (2000) 121–138.
[78] K. Yao, V. De Luca, N. Brisson, Creation of a metabolic sink for tryptophan alters the phenylpropanoid pathway and the susceptibility of potato to *Phytophthora infestans*, Plant Cell 7 (1995) 1787–1799.
[79] E.A. Maher, N.J. Bate, W. Ni, Y. Elkind, P.A. Dixon, C.J. Lamb, Increased disease susceptibility of transgenic tobacco plants with suppressed levels of preformed phenylpropanoid products, Proc. Natl. Acad. Sci. U. S. A. 91 (1994) 7802–7806.